www.gondwanags.org.in
Research Article

ISSN : 2455-1953
JGSR
Journal of Geosciences Research
Vol. 11, No.1, January, 2026, pp. 33-42

Petrographic Characteristics and Dynamic Recrystallization of Four Quartzite Units of the Central Nepal, Lesser Himalaya

Dinesh Raj Sharma and Naresh Kazi Tamrakar*

Central Department of Geology, Tribhuvan University, Kirtipur, Kathmandu, Nepal
*(*Corresponding Author, E-mail: naresh.tamrakar@cdgl.tu.edu.np)*

Abstract

Petrographic investigations of quartzites from four distinct units Fagfog, Dunga, Pandrang, and Chisapani Quartzites within the Central Nepal Lesser Himalaya were undertaken to characterize composition, texture and microstructures. The Fagfog and Dunga Quartzite respectively belong to the Lower Nawakot Group and the Upper Nawakot Group, whereas the Pandrang and the Chisapani Quartzites belong to the Bhimphedi Group of the Kathmandu Complex, and occur in ascending order. The Kathmandu Complex (allochthonous sequence) thrusts over the Nawakot Complex (autochthonous sequence) along the Mahabharat Thrust. Microscopic techniques, including polarized light microscopy and point-count analysis were employed to reveal significant petrographic variations among the studied units. The Fagfog Quartzite, comprising 89-94% quartz with minor muscovite and biotite, exhibits a massive microstructure characterized by subequant to elongate grains and evidence of low-temperature deformation dominated by subgrain rotation, indicating a sedimentary protolith with minimal metamorphic overprint. The Dunga Quartzite, containing 85-93% quartz, displays both banded and massive textures with equigranular to porphyroclastic grains, reflecting mixed recrystallization mechanisms such as subgrain rotation and grain boundary migration that suggest moderate deformation. In contrast, the Pandrang Quartzite, with quartz content ranging from 83-95%, is characterized by polygonal grains indicative of high-temperature grain boundary migration, and whereas the Chisapani Quartzite, exhibiting 85-91% quartz, is marked by ribbon-like quartz fabrics formed under intense strain at high temperatures. These petrographic differences delineate an inverted metamorphic gradient, underscoring the region's complex tectonic evolution and providing insights into lithostratigraphic correlations and potential applications as ballast material for infrastructure development. This study not only delineates quartzite petrographic variations but also enhances understanding of the regional tectono-metamorphic framework. Analysis of microstructures and mineralogical data supports inferences regarding deformation-related microfabric development and prevailing metamorphic conditions, offering valuable insights for geological research and engineering applications

Keywords: Quartzite, Petrography, Deformation, Metamorphism, Lesser Himalaya

Introduction

Quartzite is a silica-rich, durable lithology formed through either the metamorphic recrystallization of quartzose sandstones or the diagenetic cementation of quartz grains in sedimentary environments (Passchier and Trouw, 2010; Trouw *et al.*, 2010). As a rock type, quartzite is primarily composed of quartz (SiO_2), which typically accounts for over 90% of its mineralogical composition, with minor amounts of feldspar, mica, and accessory minerals such as zircon, tourmaline, and rutile (Blatt and Tracy, 1996). The high quartz content imparts exceptional hardness and resistance to weathering, making quartzite a significant rock in both geological studies and engineering applications (Sharma and Tamrakar, 2023). Quartzites in nature are classified into two primary genetic types: sedimentary quartzite (orthoquartzite) and metamorphic quartzite (metaquartzite) (Dhital, 2015; Vernon, 2018). Orthoquartzite is a sedimentary rock formed by the silica cementation of well-sorted, rounded quartz grains, preserving primary sedimentary features such as cross-bedding and grain sorting (Blatt and Tracy, 1996). In contrast, metaquartzite forms through dynamic or thermal metamorphism, leading to the recrystallization of quartz grains and the development of granoblastic textures, sutured grain boundaries, and a more interlocking crystalline structure (Stipp *et al.*, 2002). These differences are crucial for interpreting provenance and tectonic histories, as sedimentary quartzites tend to fracture around quartz grains, while metamorphic quartzites display fractures that cut through grains due to their recrystallized nature (Vernon, 2018). A key process influencing metamorphic quartzite formation is dynamic recrystallization, which involves deformation-driven reorganization of quartz grains under metamorphic conditions (Stipp *et al.*, 2010; Law, 2014). This process occurs through three progressive mechanisms: bulging recrystallization (BLG) at temperatures of 250-400°C, subgrain rotation (SGR) between 400-500°C, and grain boundary migration (GBM) above 500°C, each contributing to the development of strain-free quartz grains and modifying the rock's microstructure (Stipp *et al.*, 2002). The study

(Received : 01 July 2025 ; Revised Form Accepted : 20 November 2025)
https://doi.org/10.56153/g19088-025-0268-93

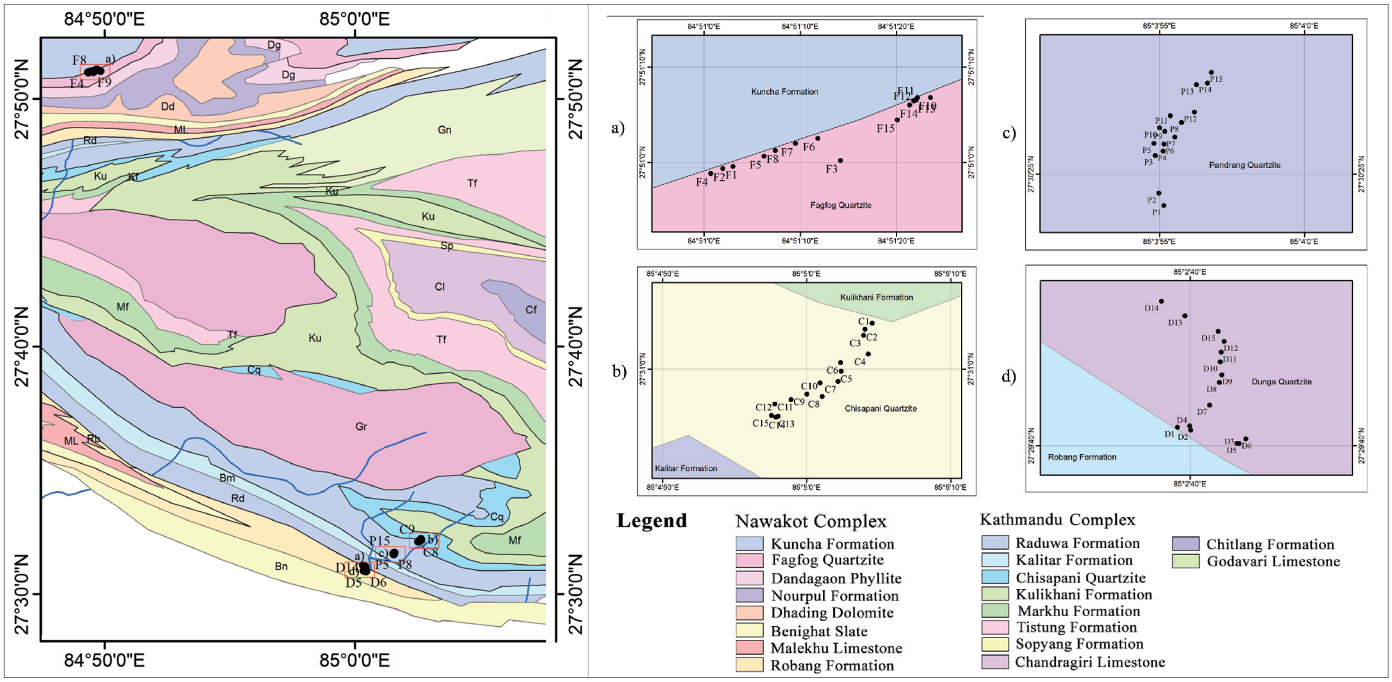

Fig.1. Geological map of study area with sampling locations

of these microstructural changes is essential for understanding deformation mechanisms and evaluating the physical properties of quartzite in various applications.

The Central Nepal Lesser Himalaya contains several significant quartzite formations that provide valuable geological and geotechnical insights (Dhital, 2002, 2015). Among these, four quartzite units the Fagfog Quartzite, Dunga Quartzite (part of the Robang Formation), Pandrang Quartzite (part of the Kalitar Formation), and Chisapani Quartzite exhibit distinct petrographic properties that influence their suitability for various applications, including use as ballast materials in railway infrastructure (Sharma and Tamrakar, 2023). While the Fagfog and Pandrang Quartzites are predominantly metamorphic, showing porphyroblastic textures, the Chisapani Quartzite is a sedimentary orthoquartzite retaining primary sedimentary features. The Dunga Quartzite presents an intermediate nature, containing interbedded phyllites and alternating silica-cemented and recrystallized layers. The primary objective of this research is to conduct a comparative petrographic analysis of these four quartzite units, focusing on their composition, texture, and microstructure. By integrating modal mineralogy with thin-section analysis, this study aims to: (1) characterize the mineralogical and textural differences among these quartzites, (2) distinguish between their sedimentary and metamor-phic origins, and (3) evaluate the role of dynamic recrystallization in shaping their petrographic attributes. This research contributes to refining lithostratigraphic correlations in the Himalayan region and provides insights into the mechanical performance of quartzite as a ballast material in infrastructure development.

Geological Setting

The study area located in the Central Nepal Himalaya, falls within the Lesser Himalaya and comprises two major geological units: the Nawakot Complex and the Kathmandu Complex, separated by the Mahabharat Thrust (Fig.1; Stöcklin and Bhattarai, 1977; Stöcklin, 1980). The Lesser Himalaya is bounded by the Main Boundary Thrust (MBT) in the south and the Main Central Thrust (MCT) in the north. The Nawakot Complex is subdivided into the Lower and Upper Nawakot Groups, predominantly composed of low-grade metasedimentary rocks (Stöcklin and Bhattarai, 1977). The Lower Nawakot Group consists of the Kuncha Formation, Fagfog Quartzite, Dandagaon Phyllite, Nourpul Formation, and Dhading Dolomite. The Kuncha Formation, the oldest unit, comprises phyllite, quartzitic phyllite, and schist (Pécher, 1978; Stöcklin, 1980; Sharma and Kizaki, 1989). The Fagfog Quartzite is characterized by milky orthoquartzite with sedimentary structures such as cross-bedding and ripple marks (Pécher, 1978; Stöcklin, 1980; Arita, 1983; Sakai, 1985; Sharma and Kizaki, 1989). The Upper Nawakot Group includes the Benighat Slate, Malekhu Limestone, and Robang Formation. The Benighat Slate and Malekhu Limestone display intercalated carbonate layers indicating a transition from deeper marine to shallow conditions (Rai, 2011). The Robang Formation consists of schist, phyllite, quartzite, and metabasic rocks, with the Dunga Quartzite as a key member.

The Kathmandu Complex consists of the Bhimphedi and Phulchauki Groups. The Bhimphedi Group, of Precambrian age, comprises higher-grade metamorphic rocks including the Raduwa Formation, Bhainsedobhan Marble, Kalitar Formation, Chisapani Quartzite, Kulikhani Formation, and Markhu Formation. The Raduwa Formation contains garnet-bearing mica schist, while the Bhainsedobhan Marble consists of coarsely crystalline marble (Stöcklin, 1980). The Kalitar Formation includes greenish-grey mica schist, and the Chisapani Quartzite is marked by fine-grained quartzite with cross-bedding and ripple marks, indicative of shallow water deposition (Stöcklin, 1980). The Kulikhani Formation consists of biotite-rich schist, quartzite, and augen gneiss, with distinct microfolds. The Markhu Formation features mixed lithology with dominant white to pink marble intercalated with schist and quartzite. This stratigraphic framework, shaped by tectonic thrusting and varied depositional environments, highlights the complex geological evolution of the Lesser Himalayan sequence (Stöcklin, 1980).

Methodology

Sample Preparation

Rock samples and quartzite gravels were collected and prepared for microscopic analysis. Each sample was cut into thin sections to facilitate observation under a polarizing microscope (Olympus POS). The thin sections were polished to ensure accurate optical analysis of mineral compositions, textures, and microstructures.

Megascopic Examination

Before microscopic analysis, a megascopic examination was conducted to analyze the physical characteristics of the rock samples. This included the identification of minerals based on visible traits such as color, luster, and crystal habit. The texture, ranging from coarse- to fine-grained, and structural features such as foliation and banding, were also assessed to determine the alignment of minerals due to metamorphic processes. Microscopic examination was conducted using a polarizing microscope under varying magnifications (7×4, 7×10, 10×4, and 10×10). This detailed analysis included:

Compositional Analysis

A point count method was used to determine the mineral composition of each thin section.

Microstructural Observations

Grain size, shape, and boundaries were examined. Mineral grains were categorized as euhedral, subhedral, or anhedral based on their crystal development.

Measurement of Mica and Non-Mica Thickness

The thickness of mica and non-mica minerals was measured to assess deformation characteristics.

Dynamic Recrystallization Analysis

The microstructural features related to dynamic recrystallization were studied to understand the deformation mechanisms within the rock samples. Three primary recrystallization mechanisms were analyzed:

Bulging Recrystallization (BLG)

Occurs at lower temperatures (~250°C to 400°C), where new small grains form along grain boundaries due to strain.

Subgrain Rotation Recrystallization (SGR)

Occurs at moderate temperatures (~400°C to 500°C), where misoriented subgrains rotate and develop into distinct grains.

Grain Boundary Migration (GBM)

Occurs at higher temperatures (~500°C to 600°C), characterized by the movement of grain boundaries, leading to the formation of larger grains with straight boundaries.

Graphical Representation

Figures 2 and 3 illustrate the relationships between temperature and recrystallized grain size, as well as the relationship between temperature and distance in dynamic recrystallization processes:

Figure 2 displays the relationship between temperature and recrystallized grain size, showing the transitions between BLG, SGR, and GBM mechanisms. Data points differentiate between grain long axis (solid circles) and short axis (open circles), with error bars indicating measurement uncertainties.

Figure 3 represents the relationship between temperature and distance, marking the transitions between recrystallization mechanisms. It highlights key mineralogical changes such as the presence of chlorite (Chl) and potassium feldspar (Kfs) at the

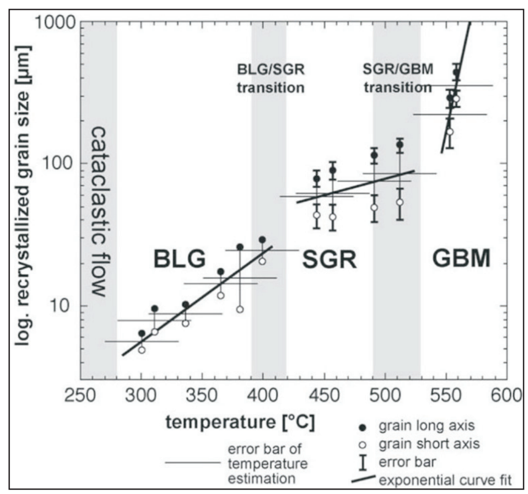

Fig.2. Temperature-distance profile showing transitions between BLG, SGR, and GBM deformation (Stipp *et al.*, 2002)

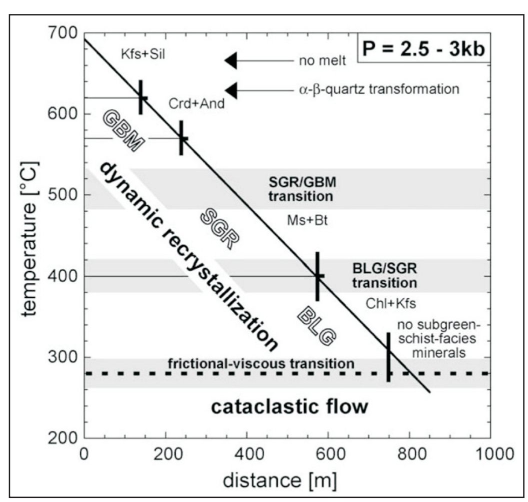

Fig.3. Relationship between temperature and recrystallized grain size, showing transitions between BLG, SGR, and GBM deformation mechanisms (Stipp *et al.*, 2002)

BLG/SGR transition, and muscovite (Ms) and biotite (Bt) at the SGR/GBM transition. The diagram also identifies the frictional-viscous transition near 300°C, distinguishing between brittle and ductile deformation.

Results

Megascopic Description

The Fagfog Quartzite is predominantly massive with a rough texture and varies in color from yellowish white to brownish white (Table 1). Some samples exhibit laminated structures. The Dunga Quartzite is primarily well-banded with a rough texture, displaying colors ranging from grey to milky white, though some occurrences are crudely banded or massive (Table 1). The Pandrang Quartzite is mainly massive with a rough texture, characterized by greenish white to dark grey hues, with occasional laminated structures and minor schist partings. The Chisapani Quartzite is mostly laminated with a rough texture, displaying light greenish grey to greenish grey colors, though some sections appear massive (Table 1).

Table 1: Megascopic description of samples studies

Unit	Sample no.	Outcrop description	Thickness of Bed	Surface Texture	Colour	Monomictic/ Polymictic	Description
Fagfog Quartzite	F1	Ripple laminated, med.-grained	4-6 m. No associated rock.	Rough	Yellowish white	Monomictic	Laminated
	F2	Ripple marks medium-grained	3-5 m. No associated rock	Rough	Brownish white	Monomictic	Massive
	F3	Ripple marks medium-grained	3-5m No associated rock.	Rough	Brownish white	Monomictic	Massive
	F4	Ripple marks medium-grained	4-6 m No associated rock.	Rough	Yellowish white	Monomictic	Massive
	F5	Ripple marks medium-grained	3-5 m No associated rock.	Rough	Yellowish white	Monomictic	Laminated
	F6	Ripple marks medium-grained	4-5 m No associated rock.	Rough	Brownish white	Monomictic	Massive
	F7	Ripple marks medium grained	8-10 m. No associated rock.	Rough	Brownish white	Monomictic	Massive
	F8	Ripple marks medium grained	3-5 m. No associated rock	Rough	White	Monomictic	Massive
	F9	Ripple marks medium-grained	3-5 m. No associated rock	Rough	Brownish white	Monomictic	Massive
	F10	Ripple marks medium-grained	3-6 m. No associated rock	Rough	White	Monomictic	Massive
	F11	Ripple marks medium-grained	2-4 m. No associated rock	Rough	White	Monomictic	Massive
	F12	Ripple marks medium-grained	2-4 m. No associated rock	Rough	Brownish white	Monomictic	Massive
	F13	Ripple marks medium-grained	3-4 m. No associated rock	Rough	White	Monomictic	Massive
	F14	Ripple marks medium-grained	2-3 m. No associated rock	Rough	Brownish white	Monomictic	Massive
	F15	Ripple marks medium-grained	3-5 m. No associated rock	Rough	White	Monomictic	Laminated
Dunga Quartzite	D1	Fine grained white	3-5 m. No associated rock.	Rough	Grey	Monomictic	Well banded
	D2	Fine grained white	3-5 m. No associated rock.	Rough	Light grey	Monomictic	Crudely banded
	D3	Fine grained white	3-5 m. No associated rock.	Rough	Grey	Monomictic	Well banded
	D4	Fine grained white	3-7 m. No associated rock.	Rough	Grey	Monomictic	Well banded
	D5	Fine grained white	2-3 m. No associated rock.	Rough	Grey	Monomictic	Well banded
	D6	Fine grained milky white	2-3 m. No associated rock.	Rough	Light grey	Monomictic	Well banded
	D7	Fine grained milky white	3-5 m. No associated rock.	Rough	Milky white	Monomictic	Crudely banded
	D8	Fine grained light grey white	3-4 m. No associated rock.	Rough	Light grey	Monomictic	Massive
	D9	Fine grained light grey white	3-4 m. No associated rock.	Rough	Milky white	Monomictic	Massive
	D10	Fine grained bluish grey white	5-7 m. No associated rock.	Rough	Milky white	Monomictic	Massive
	D11	Fine grained bluish grey white	5-8 m. No associated rock.	Rough	Milky white	Monomictic	Massive
	D12	Fine grained bluish grey white	2-5 m. No associated rock.	Rough	Milky white	Monomictic	Massive
	D13	Fine grained light grey white	3-5 m. No associated rock.	Rough	Milky white	Monomictic	Massive
	D14	Fine grained light grey white	2-3 m. No associated rock.	Rough	Milky white	Monomictic	Massive
	D15	Fine grained greenish grey white	1-2 m. No associated rock.	Rough	Milky white	Monomictic	Massive
Pandrang Quartzite	P1	Fine grained bluish grey	2-4 m. Associate rock is greenish grey micaceous schist	Rough	Greenish white	Monomictic	Massive
	P2	Fine grained gray colour	2-4 m. No associated rock.	Rough	Dark grey	Monomictic	Massive
	P3	Fine grained gray colour	4-5 m. No associated rock.	Rough	Greenish white	Monomictic	Massive
	P4	Fine grained grey colour	3-7 m. No associated rock.	Rough	Greenish white	Monomictic	Massive
	P5	Fine grained gray colour	3-5 m. No associated rock.	Rough	Greenish white	Monomictic	Massive
	P6	Fine grained bluish greenish grey	4-5 m. No associated rock.	Rough	Greenish white	Monomictic	Massive
	P7	Fine grained bluish to greenish grey	2-4 m. No associated rock.	Rough	Greenish white	Monomictic	Massive
	P8	Fine grained grey white	3-5 m. Parting of Schist.	Rough	Greenish white	Monomictic	Massive
	P9	Fine grained light grey white	2-3 m. No associated rock. Small parting of schist	Rough	Greenish white	Monomictic	Laminated
	P10	Fine grained grey colored	2-3 m. Parting of Schist	Rough	Greenish white	Monomictic	Massive
	P11	Fine grained grey colored	5-8 m. No associated rock.	Rough	Greenish white	Monomictic	Laminated
	P12	Fine grained bluish grey coloured	2-3 m. No associated rock.	Rough	Greenish white	Monomictic	Massive
	P13	Fine grained	1-2 m. No associated rock.	Rough	Greenish white	Monomictic	Massive
	P14	Fine grained grey	3-5 m. No associated rock.	Rough	Greenish white	Monomictic	Massive
	P15	Fine grained grey	0-3 m. No associated rock.	Rough	Greenish white	Monomictic	Massive
Chisapani Quartzite	C1	Fine grained grey	2-3 m. Parting of schist	Rough	Light greenish grey	Monomictic	Massive
	C2	Fine grained light grey colour	2-5 m. thin parting of schist.	Rough	Light greenish grey	Monomictic	Laminated
	C3	Fine grained light gray colour	1-2 m. No associated rock.	Rough	Light greenish grey	Monomictic	Laminated
	C4	Fine grained bluish grey colour	2-4 m. No associated rock.	Rough	Light greenish grey	Monomictic	Laminated
	C5	Fine grained gray colour	1-3 m. No associated rock.	Rough	Greenish grey	Monomictic	Massive
	C6	Fine grained light grey	1-3 m. No associated rock.	Rough	Light greenish grey	Monomictic	Laminated
	C7	Fine grained light grey	3-5 m. No associated rock.	Rough	Light greenish grey	Monomictic	Laminated
	C8	Fine grained light grey	2-3 m. No associated rock.	Rough	Light greenish grey	Monomictic	Massive
	C9	Fine grained grey	3-5 m. No associated rock.	Rough	Greenish grey	Monomictic	Massive
	C10	Fine grained light grey colored	4-5 m. No associated rock.	Rough	Light greenish grey	Monomictic	Laminated
	C11	Fine grained light grey colored	2-4 m. No associated rock.	Rough	Light greenish grey	Monomictic	Laminated
	C12	Fine grained grey colored	2-4 m. No associated rock.	Rough	Light greenish grey	Monomictic	Laminated
	C13	Fine grained light gray	3-5 m. No associated rock.	Rough	Greenish grey	Monomictic	Laminated
	C14	Fine grained light grey	3-5 m. No associated rock.	Rough	Light greenish grey	Monomictic	Laminated
	C15	Fine grained greyish white	2-3 m. No associated rock.	Rough	Light greenish grey	Monomictic	Laminated

Mineral Composition

Mineral composition of quartzite samples from study area is represented in Table 2. The Fagfog Quartzite consists predominantly of quartz (89-94%), with minor muscovite (2-6%), biotite (1-3%), and opaque/non-opaque heavies (1-3%). The Dunga Quartzite contains 85-93% quartz, with muscovite (1-8%), feldspar (up to 5%), biotite (1-5%), and heavies (1-3%). The Pandrang Quartzite has 83-95% quartz, muscovite (2-7%), feldspar (1-7%), sericite (1-5%), and minor heavies. The Chisapani Quartzite comprises 85-91% quartz, muscovite (3-5%), feldspar (3-6%), sericite (1-6%), and minor heavies. The mineralogical and textural observations clearly differentiate the four quartzite units. The Fagfog Quartzite shows high quartz purity (89-94%) with minimal feldspar and mica,

Table 2: Mineral composition of quartzite samples from study area

Stratigraphic unit	Sample	Mineral constituents, %									
		Quartz	Feldspar	Muscovite	Sericite	Biotite	Chlorite	Non-Opaque Heavies	Opaque Heavies	Other	Total
Fagfog Quartzite	F1	91			5	2		1		1	100
	F2	91			3	2		1		3	100
	F3	94			2	1	2			1	100
	F4	92			5	1		1		1	100
	F5	91			5	2		1		1	100
	F6	90			6	2		1		1	100
	F7	93			4	1		1		1	100
	F8	90			5	1	2	1		1	100
	F9	90			4	1	1	1		3	100
	F10	92			4	1	3				100
	F11	92			5	1	1	1			100
	F12	91			5	3		1			100
	F13	91			5	1		1		2	100
	F14	89			6	1	1	1		2	100
	F15	91			6	1		1		1	100
Dunga Quartzite	D1	90		1	3		4		2		100
	D2	93		2	2		2		1		100
	D3	90		3	2		3		1		100
	D4	90		3	2		2	1	2		100
	D5	85		5	2		5		3		100
	D6	93		2	2		2		1		100
	D7	92		2	5		1		1		100
	D8	92			6		1		1		100
	D9	93			6		1		1		100
	D10	90			8		1		1		100
	D11	90		2	7				1		100
	D12	93			6				1		100
	D13	91			8				1		100
	D14	90			2		3		5		100
	D15	92			6		2				100
Pandrang Quartzite	P1	90		2	7				1		100
	P2	92		1	6				1		100
	P3	91		2	7				1		100
	P4	91		2	6				1		100
	P5	91		2	6				1		100
	P6	91		2	6	1			1		100
	P7	85		3	5	5					100
	P8	95		1	3				1		100
	P9	91		2	4	2			1		100
	P10	85		4	5	1			2		100
	P11	89	1	4	5				1		100
	P12	92		2	5				1		100
	P13	91		2	6				1		100
	P14	83		7	5	4			1		100
	P15	86	1	2	4	5			1		100
Chisapani Quartzite	C1	86		5	4	4			1		100
	C2	85		5	3	4			2		100
	C3	86		3	5	5			1		100
	C4	91		5	3				1		100
	C5	90		6	3				1		100
	C6	87		6	4			1	2		100
	C7	86		3	3	6		1	1		100
	C8	89		6	3	1			1		100
	C9	88		4	3	4			1		100
	C10	90		4	3	2			1		100
	C11	86		5	3	5			1		100
	C12	88		5	3	3			1		100
	C13	88		4	4	3			1		100
	C14	90		4	3	3			1		100
	C15	87		5	4	3			1		100

dominated by subequant to elongate grains. These characteristics, along with limited mica-rich layering, support its origin as a relatively mature orthoquartzite with minimal metamorphic overprint. The Dunga Quartzite shows a wider mineralogical range (85-93% quartz) and more frequent mica-rich bands, producing well-defined compositional layering and equi-granular. These attributes reflect a mixed sedimentary metamorphic history, where primary layering is moderately modified by deformation.

The Pandrang Quartzite is texturally distinct, with polygonal and equant grains showing well-developed triple junctions, indicative of higher-temperature static and dynamic recrystallization. The Chisapani Quartzite possesses ribbon like quartz and straight grain boundaries, implying metamorphic modification of an originally orthoquartzite protolith.

Texture and Microstructure

The computed band ratios, expressed as the mode of non-mica thickness divided by the mode of mica thickness, show distinct microstructural characteristics among the quartzite samples (Fig. 4 a-d; Table 3). In the Fagfog Quartzite (Fig. 4a), the band-thickness ratios show moderate variability, reflecting relatively uniform recrystallization fabrics. In the Dunga Quartzite (Fig. 4b), the ratios range from a low of 3 to a high of 10, with many values clustering around 7 to 9. The Pandrang Quartzite (Fig. 4c) exhibits a broader spread, with ratios varying from 1 to an exceptional 25, while several samples fall within the moderate range of 3 to 11. The Chisapani Quartzite (Fig. 4d) generally displays moderate values ranging from 4 to 15, most commonly between 5 and 8.

Discussion

The Fagfog and Dunga Quartzites contain moderately high quartz contents but differ texturally. The Fagfog Quartzite preserves massive porphyroblastic fabrics with limited mica, whereas the Dunga Quartzite shows alternating mica-rich and quartz-rich bands, reflecting a stronger imprint of deformation. The Pandrang Quartzite contains polygonal grains and straight grain boundaries, suggesting recrystallization under higher temperatures, whereas the Chisapani Quartzite, though texturally laminated, frequently shows ribbon-quartz and polygonal fabrics. These distinctions show that mineralogical purity alone does not control microstructural development instead, the interplay of deformation intensity, metamorphic temperature, and sedimentary layering governs the petrographic variability among these units. The Fagfog Quartzite, characterized by ripple marks, lamination, and subequant grains, represents a sedimentary orthoquartzite with limited metamorphic modification. The Dunga Quartzite shows mixed features primary banding inherited from sedimentary layering combined with moderate metamorphic recrystallization. The Pandrang Quartzite shows hallmark features of metaquartzite, including equant polygonal grains and grain boundary mobility, reflecting deeper burial and high-grade metamorphic conditions. The Chisapani Quartzite show both sedimentary lamination and metamorphic fabrics, suggesting it originated as an orthoquartzite but experienced substantial tectonic reworking. Fagfog Quartzite show bulging and limited subgrain rotation, indicating deformation temperatures below ~450°C. The Dunga Quartzite shows subgrain rotation and locally grain boundary migration, suggesting moderate

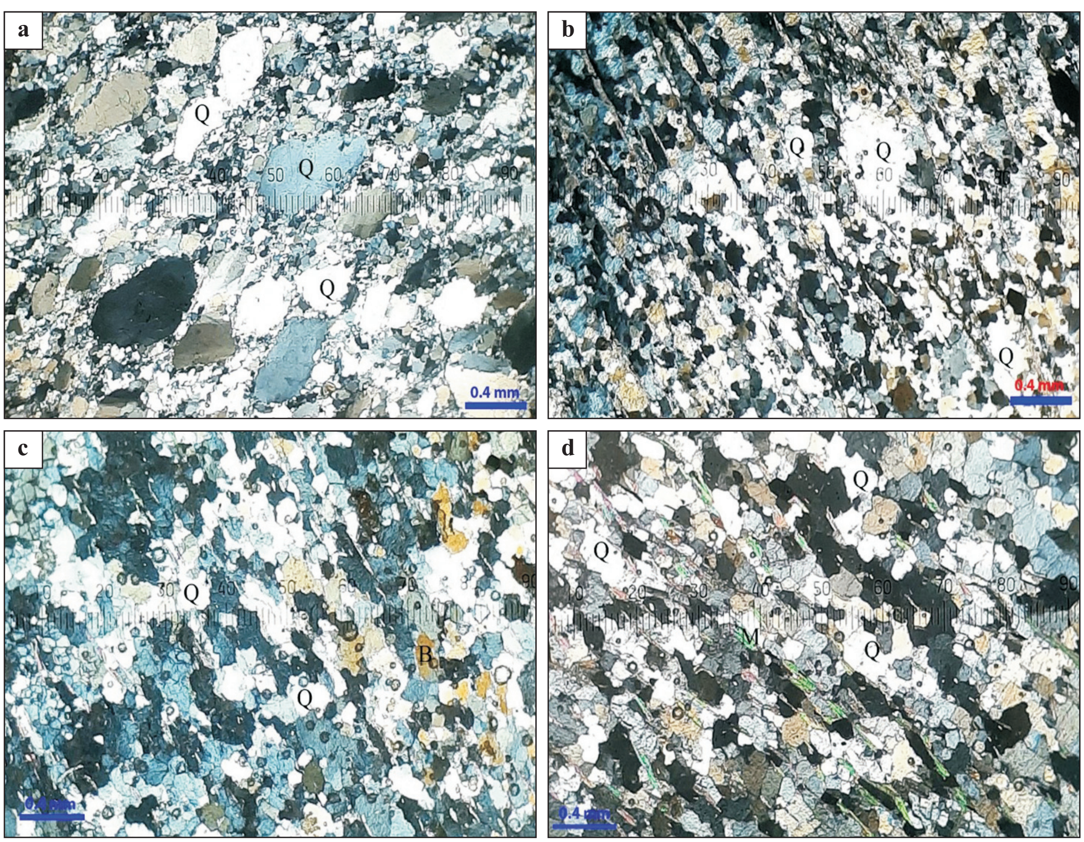

Fig.4. Microphotographs under cross-polarized light showing a) angular to sub-angular quartz grains (Q) (sample F1), b) elongated and sutured quartz grains (Q) (sample D15), c) fine- to medium-grained quartz (Q) (sample P7) and d) fine- to medium-grained quartz (Q) (Sample C14). Scale bar = 0.4 mm.

Table 3: Microfabric of quartzites in study area

Stratigraphic unit	Sample	*Quartz grain habit and fabric	Grain size (μ)				*Microstructure	**Non mica/ mica Band Ratio
			Min	Max	Avg	Mode		
Fagfog Quartzite	F1	Subequant to elongate, irregular; long to sutured	30	70	48	40	Massive, undulosed, SGR	-
	F2	Subequant to elongate, irregular; long to sutured	20	90	52	40	Massive, undulosed, SGR	-
	F3	Subequant to elongate, irregular; long to sutured	20	70	41	30	Massive, undulosed, SGR	-
	F4	Subequant to elongate, irregular; long to sutured	30	90	47	50	Massive, undulosed, SGR	-
	F5	Subequant, irregular; sutured	30	100	52	40	Massive, undulosed, BGR with minor SGR	-
	F6	Subequant to elongate, irregular; long to sutured	20	70	44	40	Massive, undulosed,, BGR with minor SGR	-
	F7	Subequant to elongate, irregular; long to sutured	20	110	46	30	Massive, undulosed, SGR	-
	F8	Subequant to elongate, irregular; long to sutured	20	110	49	30	Massive, undulosed, minor BGR with SGR	-
	F9	Subequant to elongate, irregular; long to sutured	30	110	45	50	Massive, undulosed, SGR	-
	F10	Subequant to elongate, irregular; long to sutured	30	110	51	50	Massive, undulosed, BGR with SGR	-
	F11	Subequant to elongate, irregular; long to sutured	30	90	47	40	Massive, undulosed, SGR	-
	F12	Subequant to elongate, irregular; long to sutured	30	100	49	40	Massive, undulosed, SGR	-
	F13	Subequant to elongate, irregular; long to sutured	20	110	42	40	Massive, undulosed, SGR	-
	F14	Subequant to elongate, angular to subangular; irregular; long to sutured	30	90	43	30	Massive, undulosed, minor BGR with SGR	-
	F15	Subequant to elongate, long to sutured	30	110	53	40	Massive, undulosed, minor BGR with SGR	-
Dunga Quartzite	D1	Equigranular, straight to irregular, polygonal few suture and diffused	30	100	48	40	Mica: 0.025 mm (mode); Non mica: 0.175 mm (mode)	7
	D2	Equigranular, straight to irregular, polygonal few suture and diffused	30	70	36	30	Mica: 0.020 mm; Non mica: 0.200 mm	10
	D3	Equigranular, straight to irregular, polygonal few suture and diffused, few elongated grains	30	70	38	60	Mica: 0.020 mm; Non mica: 180 m	9
	D4	Equigranular, small subgrain, equant subgrain, mostly irregular, and ameobodial	30	110	46	60	Mica: 0.015 mm; Non mica: 0.181 mm	10
	D5	Equigranular, small subgrain, equant subgrain, mostly irregular, and ameobodial	30	90	41	40	Mica: 0.015 mm; Non mica: 0.100 mm	7
	D6	Equigranular, small subgrain, equant subgrain, mostly irregular, and ameobodial	30	90	35	30	Mica: 0.030 mm; Non mica: 120 mm	4
	D7	Equigranular, small subgrain, equant subgrain, mostly irregular, and ameobodial	20	60	39	40	Mica: 0.030 mm; Non mica: 0.080 mm	3
	D8	Equigranular, small subgrain, equant subgrain, mostly irregular, ameobodial, and slightly diffused boundary	30	90	43	50	Mica: 0.030 mm; Non mica: 0.120 mm	4
	D9	Dynamic recrystalization, small subgrain to large pophyro clast, with irregular boundaries, and ameobodial habit	30	130	80	60	Mica: 0.030 mm; Non mica: 0.275 mm	9
	D10	Dynamic recrystalization, small subgrain to large pophyro clast, with irregular boundaries, ameobodial habbit, more elongated and lensolidal shape	30	110	57	40	Mica: 0.020 mm; Non mica: 150 mm	8
	D11	Dynamic recrystalization with distinct folliation, equigranular, few lensolidal, irregular, and suture boundary	20	100	56	40	Mica: 0.035 mm; Non mica: 0.100 mm	3
	D12	Equigranular, notable subgrain proportion nearby 50%, and irregular boundary	30	130	62	70	Mica: 0.030 mm; Non mica: 0.120 mm	4
	D13	Slightly equigranular, irregular, suture, diffused grain boundary with few elongated grain	30	130	52	40	Mica: 0.015 mm; Non mica: 0.090 mm	6
	D14	Equigranular, irregular suture, and diffused with few elongated grains.	20	70	42	30		
	D15	Less equigranular, irregular diffuse, boundary among grains, and moreless subequant	30	130	61	40	Mica: 0.015 mm; Non mica: 0.100 mm	7
Pandrang Quartzite	P1	Subequant, straight to irregular grain boundary	20	80	47	40	Mica: 0.010 mm; Non mica: 0.250 mm	25
	P2	Subequant, few elongate, straight to irregular boundary	30	170	73	70	Mica: 0.030 mm; Non mica: 0.325 mm	11
	P3	Subequant, irregular to straight polygonal	20	150	64	70	Mica: 0.050 mm; Non mica: 0.350 mm	7
	P4	Subequant, irregular to straight polygonal	30	130	65	50	Mica: 0.020 mm; Non mica: 0.080 mm	4
	P5	Subequant, irregular to straight polygonal	30	90	53	40	Mica: 0.035 mm; Non mica: 0.100 mm	3
	P6	Subequant, irregular to straight polygonal	30	120	69	60	Mica: 0.025 mm; Non mica: 0.275 mm	11
	P7	Subequant, irregular to straight polygonal	30	110	64	50	Mica: 0.030 mm; Non mica: 0.160 mm	5
	P8	Subequant, irregular to straight polygonal	30	110	51	40	Mica: 0.015 mm; Non mica: 0.140 mm	9
	P9	Equigranular, equant, few elongate, straight to irregular	30	110	58	40	Mica: 0.015 mm; Non mica: 0.050 mm	3
	P10	Equigranular, subequant, elongate, Straight to irregular	20	100	50	40	Mica: 0.040 mm; Non mica: 0.210 mm	5
	P11	Mostly equant, straight polygonal to irregular boundary	30	130	54	60	Mica: 0.055 mm; Non mica: 0.150 mm	3
	P12	Mostly equant, straight polygonal to irregular boundary	30	90	48	40	Mica: 0.040 mm; Non mica: 0.075 mm	2
	P13	Subequant, polygonal grains, mostly straight, few irregular	30	110	52	50	Mica: 0.050 mm; Non mica: 0.200 mm	4
	P14	Mostly subequant grains, polygonal, straight, few irregular	30	80	48	40	Mica: 0.050 mm; Non mica: 0.080 mm	1
	P15	Mostly subequant grains, polygonal, straight, few irregular	30	130	68	50	Mica: 0.020 mm; Non mica: 0.110 mm	6
Chisapan Quartzite	C1	Equigranular, subequant to elongate, straight to substraight	30	130	53	50	Mica: 0.020 mm; Non mica: 0.100 mm	5
	C2	Equigranular, subequant to elongate, straight to substraight, ribbon like	40	140	76	70	Mica: 0.030 mm; Non mica: 0.195 mm	7
	C3	Equigranular, subequant to elongate, straight to substraight, ribbon like	30	100	57	40	Mica: 0.030 mm; Non mica: 0.250 mm	8
	C4	Equigranular, subequant to elongate, straight to substraight, ribbon like	30	110	46	50	Mica: 0.030 mm; Non mica: 0.300 mm	8
	C5	Polygonal, three boundary junctions	20	70	36	30	Mica: 0.050 mm; Non mica: 0.300 mm	6

(Table contd. .....)

(Table contd. .....)

Stratigraphic unit	Sample	*Quartz grain habit and fabric	Grain size (μ)				*Microstructure	**Non mica/ mica Band Ratio
			Min	Max	Avg	Mode		
	C6	Equigranular, subequant to elongate, ribbon like, straight to substraight, polygonal	30	130	60	40	Mica: 0.050 mm; Non mica: 0.250 mm	5
	C7	Equigranular, subequant to elongate ribbon like quartz, straight to substraight, polygonal	30	130	79	70	Mica: 0.020 mm; Non mica: 0.160 mm	8
	C8	Equigranular, subequant to elongate ribbon like quartz, straight to substraight, polygonal	30	110	56	40	Mica: 0.030 mm; Non mica: 0.130 mm	4
	C9	Equigranular, subequant to elongate ribbon like quartz, straight to substraight, polygonal	30	110	58	50	Mica: 0.020 mm; Non mica: 0.210 mm	11
	C10	Equigranular, subequant to elongate ribbon like quartz, straight to substraight, polygonal	40	110	76	80	Mica: 0.015 mm; Non mica: 0.220 mm	15
	C11	Equigranular, subequant to elongate, straight to substraight, polygonal	40	110	69	60	Mica: 0.015 mm; Non mica: 0.200 mm	13
	C12	Equigranular, subequant to elongate ribbon like quartz, straight to substraight, distinct polygonal	30	100	57	40	Mica: 0.015 mm; Non mica: 0.150 mm	10
	C13	Equigranular, subequant to elongate ribbon like quartz, straight to substraight, distinct polygonal	30	100	62	40	Mica: 0.030 mm; Non mica: 0.200 mm	7
	C14	Equigranular, subequant to elongate, straight to substraight, polygonal	30	110	58	90	Mica: 0.025 mm; Non mica: 0.150 mm	6
	C15	More subequant than elongate, straight to substraight, distinct polygonal	30	130	77	70	Mica: 0.030 mm; Non mica: 0.200 mm	7

* Microstucture: BLG=buldging grain recrystallization; SGR=sediment grain rotation
** Band Ratio = Mode of Non-mica thickness/Mode of mica thickness

deformation typical of syn-tectonic recrystallization. The Pandrang Quartzite contains fully polygonal grains, reflecting dominant grain boundary migration at temperatures above 500°C. The Chisapani Quartzite shows ribbon-quartz and elongate grains, consistent with high-strain deformation under elevated temperatures. These variations reflect an inverted metamorphic gradient across the study area and establish dynamic recrystallization as a key mechanism shaping the petrographic attributes of the quartzite units.

The quartzites of the Alaknanda Valley including the Fagfog, Dunga, Pandrang, and the Chisapani Quartzites show a remarkably high quartz content (83-95%), reflecting their derivation from mature, well-sorted, quartz-rich sandstones that experienced extensive weathering and transport (Myrow *et al*., 2010; Gehrels *et al.,* 2011). Despite this compositional uniformity, these quartzites have distinct microstructural fabrics that mirror variations in metamorphic conditions and deformation histories. Although petrographic observations reveal subtle indicators of intracrystalline deformation such as undulose extinction, limited subgrain development, and locally irregular grain boundaries the Fagfog Quartzite overall reflects low-strain, low-grade metamorphic conditions consistent with temperatures below ~450°C (Law *et al.*, 2013; Passchier and Trouw, 2023). In contrast, the Dunga Quartzite displays more pronounced deformation features, including enhanced recrystallized grain fractions and irregular or migrating grain boundaries, suggesting spatial variations in strain intensity likely associated with thrust-related deformation processes in the Lesser Himalaya (Grujic *et al*., 2011). The Pandrang Quartzite, characterized by polygonal grains with straight boundaries, records high-temperature deformation (above 550°C) as evidenced by dynamic recrystallization processes (Stipp *et al.,* 2010; Larson *et al.,* 2013). Meanwhile, the Chisapani Quartzite features distinctive ribbon-like quartz fabrics, which underscore non-coaxial, high-strain conditions and further highlight the role of dynamic recrystallization mechanisms (Law, 2014; Mottram *et al.,* 2015). These microstructural differences illustrate an inverted metamorphic gradient, progressing from low-temperature dynamic recrystallization in the Fagfog unit to high-temperature recrystallization in the Pandrang and Chisapani units. This evolution is consistent with experimental and field observations that link deformation mechanisms such as SGR, BLG, and GBM to specific temperature and strain rate regimes (Hirth and Tullis, 1992; Passchier and Trouw, 2005). Comparable deformation processes have been documented in quartzites from other regions; for example, dynamic recrystallization fabrics similar to those in the Himalayan quartzites occur in the Bhutan Himalaya (Grujic *et al.,* 1996) and along the Alpine Fault in New Zealand (Stipp *et al.,* 2002). In addition, static recrystallization textures observed in the Himalayan quartzites bear resemblance to those reported from the Dora Maira Massif in Italy (Lenze and Stockhert, 2007) and the Ryoke Belt in Japan (Otani and Wallis, 2006).

The petrography of these Himalayan quartzites also compares well with other quartzites within India. Quartzites from the Aravalli Belt, for instance, are similarly quartz-dominated and preserve accessory minerals such as detrital zircon and rutile (Gogte and Ramana, 1982). Conversely, quartzites from the Eastern Ghats Belt often exhibit high-grade metamorphic minerals like sillimanite and feldspar, reflecting more intense metamorphic conditions (Sharma *et al.*, 2011). On a global scale, analogous microstructural processes are evident; coarse-grained quartzites that display GBM/GBAR textures (which, for example, enhance seismic velocities) have been observed in the Ivrea Zone in Italy (Parsons *et al.,* 1995). Similar GBM/GBAR textures have also been reported in the Cap de Creus mylonites in Spain (Piazolo and Passchier, 2002), further underscoring the role of high-temperature annealing in quartzite evolution. Beyond fabric characteristics, the tectonic implications of these quartzite variations are significant. The high-temperature deformation fabrics such as those documented in the Pandrang and Chisapani Quartzites are emblematic of localized high-strain conditions that have been central to channel flow and strain localization within the Himalayan orogen (Beaumont *et al.,* 2010; Kohn, 2014; Jamieson and Beaumont, 2013). Moreover, the occurrence of both dynamic (SGR, BLG) and static (GBM) recrystallization mechanisms within these units implies that variations in temperature and strain rate have played a critical role in controlling deformation localization and exhumation patterns (Kidder *et al.,* 2018; Butler *et al.,* 2024; Parsons *et al.,* 2022). In summary, while the quartzites of the Alaknanda Valley share a common, quartz-dominated composition, their accessory mineralogy and deformation fabrics reveal a complex interplay of tectonic and metamorphic processes. The continuum from low-grade SGR-dominated fabrics in the Fagfog Quartzite to high-temperature GBM features in the Pandrang and the Chisapani Quartzites reflects both regional metamorphic gradients and broader tectonic dynamics. When compared with quartzites from other parts of India and the world including those from the Aravalli and Eastern Ghats Belts, the Bhutan Himalaya, New Zealand's Alpine Fault, and various global analogs (Lenze and Stockhert, 2007) the Alaknanda quartzites underscore the universality of quartz recrystallization processes while highlighting the critical influence of local tectono-metamorphic histories (Law *et al.,* 2013; Grujic *et al.,* 2011; Stipp *et al.,* 2010; Larson *et al.,* 2013; Law, 2014; Mottram *et al.,* 2015; Passchier and Trouw, 2005).

Conclusions

The four quartzite units show clear mineralogical and textural distinctions that reflect their contrasting origins and metamorphic histories. The Fagfog Quartzite, dominated by massive porphyroblastic quartz with minor mica, represents a mature sedimentary orthoquartzite modified only by low-temperature deformation through bulging and limited sub-grain rotation. The Dunga Quartzite shows mixed sedimentary and metamorphic signatures, where mica-rich banding and equigranular to porphyroclastic grains indicate moderate recrystallization involving both SGR and localized GBM. The Pandrang Quartzite preserves the strongest metamorphic imprint, with polygonal grains and straight grain boundaries characteristic of high-temperature GBM dominated recrystallization. The Chisapani Quartzite, while retaining sedimentary lamination, displays ribbon-quartz and polygonal fabrics that reflect significant tectonic reworking under elevated strain.

Authors' Contributions

DRS: Field Sampling, Laboratory Analysis, Data Analysis, Interpretation, Writing the Original Draft of the Manuscript. **NKT:** Conceptual Framework, Supervision, Critical Review and Editing of the Original and Revised manuscript.

Conflict of Interests

The authors declare that they have no known financial or non-financial competing interests that could have influenced the work reported in this manuscript.

Acknowledgements

The research is a part of First Author's Ph.D. work at Central Department of Geology, Tribhuvan University, Kirtipur Nepal. The authors would like to thank the Central Department of Geology, Tribhuvan University for equipment and laboratory, Institute of Engineering, Tribhuvan University, and Department of Mines and Geology Government of Nepal for necessary laboratory facilities.

References

Arita, K. (1983). Origin of the inverted metamorphism of the lower Himalayas, Central Nepal. Tectonophysics, v. 95(1–2), pp. 43–60.

Beaumont, C., Jamieson, R.A. and Nguyen, M.H. (2010). Models of large, hot orogens containing a collage of reworked and accreted terranes. Canadian Jour. Earth Sci., v. 47(4), pp. 485–515.

Blatt, H. and Tracy, R.J. (1996). Petrology: Igneous, sedimentary, and metamorphic (2nd ed.). W.H. Freeman, New York.

Butler, R.W.H., Torvela, T. and Williams, L. (2024). An introduction to geological mapping of our world and others. Geol. Soc. London, Spec. Publ. 541p. https://doi.org/10.1144/SP541-2023-201

Dhital, M.R. (2002). Geology of the Nepal Himalaya: A regional perspective. Jour. Nepal Geol. Soc., v. 27, pp. 1–14.

Dhital, M.R. (2015). Geology of the Nepal Himalaya: Regional perspective of the classic collided orogen. Springer. https://doi.org/10.1007/978-3-319-02496-7

Gehrels, G.E., Kapp, P., DeCelles, P., Pullen, A., Blakey, R., Weislogel, A., Ding, L., Guynn, J., Martin, A., McQuarrie, N. and Yin, A. (2011). Detrital zircon geochronology of pre-Tertiary strata in the Tibetan-Himalayan orogen. Tectonics, v. 30(5), pp. TC5016.

Gogte, B.S. and Ramana, Y.V. (1982). Petrological characteristics of granitoids from the Himalaya. Him. Geol., v. 12, pp. 132–155.

Grujic, D., Casey, M., Davidson, C., Hollister, L.S., Kundig, R., Pavlis, T. and Schmid, S. (1996). Ductile extrusion of the Higher Himalaya. Tectonophysics, v. 260(1–3), pp. 21–43.

Grujic, D., Warren, C.J. and Wooden, J.L. (2011). Rapid synconvergent exhumation of Miocene-aged lower orogenic crust in the eastern Himalaya. Lithosphere, v. 3(5), pp. 346–366.

Hirth, G. and Tullis, J. (1992). Dislocation creep regimes in quartz aggregates. Jour. Struct. Geol., v. 14(2), pp. 145–159.

Jamieson, R.A. and Beaumont, C. (2013). On the origin of orogens. Geol. Soc. Am. Bull., v. 125(11–12), pp. 1671–1702.

Kidder, S., Hirth, G., Avouac, J.P. and Behr, W. (2018). The influence of stress history on the grain size and microstructure of experimentally deformed quartzite. Jour. Struct. Geol., v. 110, pp. 125–141.

Kohn, M.J. (2014). Himalayan metamorphism and its tectonic implications. Ann. Rev. Earth Planet. Sci., v. 42, pp. 381–419.

Larson, K.P., Godin, L. and Price, R.A. (2013). Relationships between displacement and distortion in orogens: Linking the Himalayan foreland and hinterland in central Nepal. Geol. Soc. Am. Bull., v. 125(7–8), pp. 1151–1170.

Law, R.D. (2014). Deformation thermometry based on quartz c-axis fabrics and recrystallization microstructures: A review. Jour. Struct. Geol., v. 66, pp. 129–161.

Law, R.D., Stahr, D.W., Francsis, M.K., Ashley, K.T., Grasemann, B. and Ahmad, T. (2013). Deformation temperatures and flow vorticities near the base of the Greater Himalayan Series, Sutlej Valley and Shimla Klippe, NW India. Jour. Struct. Geol., v. 54, pp. 21–53.

Lenze, A. and Stöckhert, B. (2007). Microfabrics of experimentally deformed quartz aggregates: Evidence for different deformation regimes. Jour. Struct. Geol., v.29(9), pp.1451–1466

Mottram, C.M., Warren, C.J., Regis, D., Roberts, N.M.W., Harris, N.B.W., Argles, T.W. and Parrish, R.R. (2015). Developing an inverted Barrovian sequence; insights from monazite petrochronology. Earth Planet. Sci. Lett., v. 425, pp. 161–172.

Myrow, P.M., Hughes, N.C., Goodge, J.W., Fanning, C.M., Williams, I.S., Peng, S., Bhargava, O.N., Parcha, S.K. and Pogue, K.R. (2010). Extraordinary transport and mixing of sediment across Himalayan central Gondwana during the Cambrian–Ordovician. Geol. Soc. Am.

Bull., v. 122(9–10), pp. 1660–1670.

Otani, M. and Wallis, S. (2006). Quartz lattice preferred orientation patterns and static recrystallization. Geology, v. 34(7), pp. 561–564.

Parsons, T., Christensen, N.I. and Wilshire, H.G. (1995). Velocities of southern Basin and Range xenoliths. Geology, v. 23(2), pp. 129–132.

Passchier, C.W. and Trouw, R.A.J. (2010). Microtectonics (2nd ed.). Springer, Berlin.

Passchier, C.W. and Trouw, R.A.J. (2023). Microtectonics (3rd ed.). Springer Nature, Berlin.

Pecher, A. (1978). Déformations et métamorphisme associés à une zone de cisaillement. Exemple du grand Chevauchement Central Himalayen (M.C.T.), transversale des Anapurnas et du Manaslu (Népal). Doctoral Dissertation, Université Scientifique et Médicale de Grenoble, pp. 8–19.

Piazolo, S. and Passchier, C.W. (2002). Controls on lineation development in low to medium grade shear zones. Jour. Struct. Geol., v. 24(1), pp. 25–44.

Rai, S. (2011). Lithostratigraphy of the Nawakot Complex (Lesser Himalayan Sequence) from Malekhu area (south-west) to Syabrubensi area (north-east) along the Trishuli River, central Nepal Himalaya. Jour. Nepal Geol. Soc., v. 42, pp. 65–74.

Sakai, H. (1985). Geology of the Kali Gandaki Supergroup of the Lesser Himalayas in Nepal, pp. 337–397.

Sharma, D.R. and Tamrakar, N.K. (2023). Strength and durability status of the Fagfog Quarzite from the Lower Nawakot Group, central Nepal Lesser Himalaya. Jour. Nepal Geol. Soc., v.65(1), pp. 71-88. https://doi.org/10.3126/jngs.v65i01.57753

Sharma, R., Gupta, V., Arora, B.R. and Sen, K. (2011). Petro-physical properties of the Himalayan granitoids. Tectonophysics, v. 497(1–4), pp. 23–33.

Sharma, T. and Kizaki, K. (1989). Metamorphism and thermal history of the Jaljala Synclinorium, central west Nepal Himalaya. Jour. Nepal Geol. Soc., v. 6, pp. 21–36.

Stipp, M., Stunitz, H., Heilbronner, R. and Schmid, S.M. (2002). The eastern Tonale fault zone. Jour. Struct. Geol., v. 24(12), pp. 1861–1884.

Stipp, M., Stünitz, H., Heilbronner, R. and Schmid, S.M. (2010). The eastern Tonale fault zone: A 'natural laboratory' for crystal plastic deformation of quartz over a temperature range from 250 to 700°C. Jour. Struct. Geol., v. 32(7), pp. 968–982.

Stöcklin, J. (1980). Geology of Nepal and its regional frame: Thirty-third William Smith Lecture. Jour. Geol. Soc., v. 137, pp. 1–34.

Stöcklin, J. and Bhattarai, K. (1977). Geology of Kathmandu area and Central Mahabharat range: Nepal Himalaya. Report of Department of Mines and Geology, United Nations Development Programme, 86p.

Trouw, R.A.J., Passchier, C.W. and Wiersma, D.J. (2010). Atlas of mylonites–and related microstructures. Springer, Berlin.

Vernon, R.H. (2018). A practical guide to rock microstructure (2nd ed.). Cambridge University Press, Cambridge.